Kinetics of oxidation of low-index surfaces of magnetite



2004 J. Phys.: Condens. Matter 16 1

(http://iopscience.iop.org/0953-8984/16/1/001)

INSTITUTE OF PHYSICS PUBLISHING JOURNAL OF PHYSICS: CONDENSED MATTER

J. Phys.: Condens. Matter **16** (2004) 1–12 PII: S0953-8984(04)67791-5

# Kinetics of oxidation of low-index surfaces of magnetite

**Y Zhou[1], Xuesong Jin[1], Y M Mukovskii[2] and I V Shvets[1]**

[1] SFI Nanoscience Laboratory, Trinity College, Dublin 2, Republic of Ireland
[2] Moscow State Steel and Alloys Institute, Moscow 119049, Russia

Received 19 August 2003
Published 15 December 2003
Online at stacks.iop.org/JPhysCM/16/1 (DOI: 10.1088/0953-8984/16/1/001)

**Abstract**

We report on studies of the kinetics of magnetite oxidation, focusing on the early stages of the process. In order to achieve well-defined experimental conditions, we used low-index surfaces of single crystals of magnetite: (111), (110) and (100). For this study we have developed a new technique utilizing the *in situ* hot stage of a high-resolution x-ray diffractometer. Other techniques were also employed, including Raman spectroscopy and vibrating sample magnetometry. We found that on all three surfaces a layer of haematite, $\alpha$-$Fe_2O_3$, was formed as a result of annealing at 300 °C in air. The layers of oxides formed on all three low-index surfaces of magnetite are non-epitaxial. The layer thickness was calculated as a function of annealing time. The oxidation rate for the (100) surface was significantly greater than for the other two surfaces. Parameters of the oxidation kinetics were obtained through a fitting procedure. The results suggest that the mechanisms of oxidation for these three orientations are different. The oxidation of the magnetite (110) and (111) surfaces is in line with the Wagner model, but this is not the case for the (100) surface. We consider possible mechanisms of oxidation and compare our results with the results of oxidation in powder magnetite.

## 1. Introduction

Magnetite ($Fe_3O_4$) is of interest to many scientific and technological disciplines [1]. This material has a high Curie temperature, a high degree of spin polarization and a weak magnetocrystalline anisotropy. These properties make magnetite a potential candidate for spin electronic devices such as spin valves, spin tunnel junctions and microwave resonant circuits [2–4]. Understanding surfaces and interfaces is of key importance for spin electronics as almost any spin electronic device involves at least one interface between two different materials. The application of magnetite in these fields is impeded due to the high complexity of its surfaces. The (100) surface has been studied to a greater extent than other low-index surfaces. It was found [5] that the (100) surface undergoes a metal–insulator transition above

  

room temperature, well above the Verwey temperature of 123 K, which is the temperature of the metal–insulator transition in the bulk of stoichiometric magnetite. The (111) surface is also very interesting. It has been found that at the correct value of surface stoichiometry the surface forms a regular superstructure in which the electron band is modulated through electron–lattice interaction creating a two-dimensional network of giant static polarons [6].

A well-known characteristic of the iron oxide family is the variety of possible conversions between the different phases: FeO, $Fe_3O_4$ and $Fe_2O_3$. $Fe_2O_3$ has two typical modifications: $\alpha$-$Fe_2O_3$ with a corundum structure and $\gamma$-$Fe_2O_3$ having the structure of a spinel with cationic vacancies [1]. Understanding of the oxidation kinetics in magnetite is not only important for potential applications of this material in spintronics but also for corrosion science in general, as iron oxides are fundamental for this subject. The oxidation of magnetite has been studied extensively [7–12]. Colombo *et al* [9, 10] investigated the oxidation of magnetite and considered it to be a two-stage process. The first stage in the oxidation of $Fe_3O_4$ is a single-phase topotactic reaction leading to the intermediate solid solution phase, $Fe_{3-x}O_4$. During the second stage disordered samples oxidize readily to $\gamma$-$Fe_2O_3$, and $\alpha$-$Fe_2O_3$ is formed only when $\alpha$-$Fe_2O_3$ nuclei or stacking faults are present. Gallagher *et al* [11, 12] proposed a mechanism for the oxidation of $Fe_3O_4$ based on the diffusion of iron cations. The diffusion coefficient was found to depend on the ratio of $Fe^{2+}$ to the total iron concentration. They observed that magnetite particles of size larger than about 300 nm were oxidized to $\alpha$-$Fe_2O_3$ below 180 °C. These results were contrary to the conclusions of Colombo *et al* [9, 10] who maintained that below 600 °C magnetite never oxidizes to $\alpha$-$Fe_2O_3$ unless $\alpha$-$Fe_2O_3$ nuclei are already present. Yet, no traces of $\alpha$-$Fe_2O_3$ nuclei were detected in the powder before annealing in [11] and [12]. An analysis of the published results suggests that the dynamics of oxidation of magnetite is sensitive to the purity and grain size of the sample. Most of the results published so far are based on powder or polycrystalline magnetite. The dependences of the oxidation kinetics on the crystal orientation of the magnetite surface and anisotropic iron diffusion coefficients are unclear. Yet these are essential to verify any model of phase transition kinetics in these complicated materials. In this paper on the study of magnetite oxidation dynamics, we decided to use a well-defined system: the low-index surface of a single crystal.

Several methods such as oxidation weight gain [13], x-ray powder diffraction [14] and thermomagnetic measurement [15] have been employed to study the oxidation kinetics of iron oxides. Most of these methods are not surface sensitive and are therefore unsuitable for investigation of the nanometre scale oxidation of materials. Assuming that 10 nm of magnetite transforms to haematite at the surface of a 1 mm thick single crystal, the weight gain and thermomagnetic methods should give relative changes in signal of $1.5 \times 10^{-7}$ and $1 \times 10^{-5}$ respectively. X-ray reflectivity measurements, which are surface sensitive, have been employed to study the oxidation of metals [16, 17]. However, this technique is only useful when the thickness of the oxide layer is in a certain range and the interface roughness is small.

In this paper we employed *in situ* high-resolution x-ray diffraction (HRXRD) and used a 'cap layer' model as a basis for the analysis of results. In the 'cap layer' technique we set the diffractometer to monitor one of the diffraction peaks of magnetite. The peak intensity decreases as the layer of magnetite is transformed into other oxides, forming a cap layer. The thickness of the layer transformed can be calculated from the reduction in the peak intensity. This technique offers good surface sensitivity and versatility, and provides results which are easy to interpret. The thickness of the layer transformed can be readily calculated if the linear absorption coefficient of the cap layer is known. The aim of the present work is to investigate the oxidation kinetics for low-index surfaces of magnetite single crystals. The dependences of the surface oxide layer thickness on the annealing time and temperature were obtained by means of HRXRD measurements. Parameters of the kinetics were deduced from the experimental

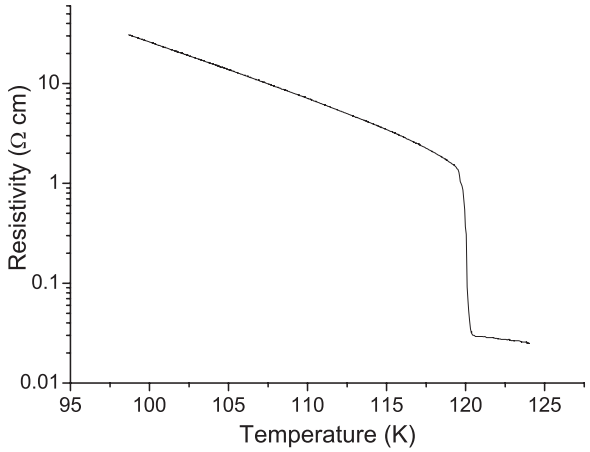


**Figure 1.** Resistivity versus temperature of the magnetite single crystal used in the experiment.

results. The possible reasons for the observed difference in the oxidation kinetics for magnetite surfaces of different crystallographic orientations are discussed.

## 2. Experimental procedures

Magnetite ($Fe_3O_4$) single crystal was grown by the floating zone technique and cut along (100), (110) and (111) planes with a precision of $\pm 1^\circ$ by spark erosion. Specimens were mechanically polished down to a 1 $\mu$m grain size. Characterization of the samples by x-ray powder diffractometry and single-crystal high-resolution diffractometry using a Cu target ($\lambda = 1.540\,56$ Å) showed good agreement with the reference peaks for magnetite. A Verwey transition temperature of 120 K was measured from the discontinuity in the resistivity versus temperature curves, shown in figure 1, indicating that the crystal is stoichiometric. Measurements of the magnetization of the samples around the Verwey transition temperature ($T_V$) were performed in fields of 5–50 mT, using a vibrating sample magnetometer. The values of the $T_V$ obtained from the magnetization and resistivity measurements were consistent. A saturation magnetization value of 94 emu $g^{-1}$, obtained from the magnetization measurements at 297 K, is consistent with the expected value for magnetite. By characterizing the sample using Raman spectroscopy measurements, we were able to positively exclude the presence of other iron oxide phases in the crystal, which are known to affect the oxidation reaction [9, 10]. Each sample was in the form of a slice of $Fe_3O_4$ some 0.5–0.7 mm thick and having lateral dimensions of 3–6 mm.

A BEDE D1 diffractometer was employed to carry out the XRD measurements. The diffractometer is equipped with one channel-cut Si crystal as a monochromator. It is further equipped with a TTK 450 Anton Paar chamber which comprised a water-cooled, vacuum-tight, stainless steel vessel with a window covered by a polymer film. This facility allowed the samples to be annealed *in situ*, without removing them from the XRD set-up. This greatly improved the accuracy of the measurements as the intensity of the beam was not affected by a possible change in sample's position: the sample position at the diffractometer was not altered during the oxidation cycle.

Here we present a model employed by us to calculate the thickness of the transformed subsurface layer. A surface layer of magnetite transforms to other oxide phases during thermal

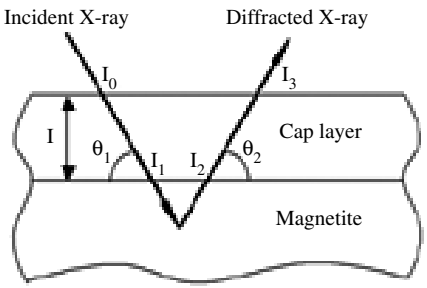


**Figure 2.** The annealing induced layer acts as a cap layer on the sample and scatters the incident and diffracted x-rays.

annealing. The annealing-induced layer acts as a cap layer on the sample and scatters the incident and diffracted x-rays, as shown in figure 2. The intensities of the incident x-ray beam before and after scattering by the cap layer are $I_0$ and $I_1$, respectively, and those of the diffracted beam before and after scattering by the cap layer are $I_2$ and $I_3$, respectively. These can be described as:

$$I_1 = I_0 \mathrm{e}^{-\mu t(\tau)/\sin\theta_1},$$
$$I_2 = C^* I_1,$$
$$I_3 = I_2 \mathrm{e}^{-\mu t(\tau)/\sin\theta_2},$$

thus

$$I_3 = C^* I_0 \mathrm{e}^{-\mu t(\tau)/\sin\theta_1 - \mu t(\tau)/\sin\theta_2}.$$

The ratio of diffracted beam intensity with and without the cap layer is

$$K(\tau) = I_3(\tau)/I_3(0) = \mathrm{e}^{-\mu t(\tau)/\sin\theta_1 - \mu t(\tau)/\sin\theta_2}. \quad (1)$$

$K(\tau)$ is a function of the annealing time $\tau$ and $\mu$ is the linear absorption coefficient of the cap layer material. It is a function of the composition of the cap layer. If the stoichiometry of the cap layer varies to such an extent that it cannot be described as comprising a dominant iron oxide phase replacing the magnetite, then strictly speaking $\mu$ is also a function of annealing time. However, to simplify the calculation, $\mu$ is thought to be time independent. The validity of this simplification is confirmed by the conclusion of the study showing that $\alpha$-$Fe_2O_3$ is the dominant phase formed at the surface during annealing. $C^*$ is a scattering factor which is a characteristic of the material forming the diffraction peak (magnetite) and the peak index, it represents the intensity ratio of the incident and diffraction beams of magnetite and is a constant. $t(\tau)$ is the cap layer thickness and is a function of annealing time. $\theta_1$ and $\theta_2$ are the angles between the incident (diffracted) beam and sample surface respectively. Therefore, dependence of the cap layer thickness $t$ can be calculated from equation (1).

Before the samples were annealed, a symmetric $\omega$–$2\theta$ scan around the (400), (440) and (222) Bragg peaks was performed for the (100), (110) and (111) samples respectively. The magnetite single crystals were then annealed under an air atmosphere for the required time at temperatures of up to 300 °C. The chamber was then pumped, to a pressure of less than 1 Pa, to prevent further oxidation of the sample and a further XRD measurement was performed. After the XRD measurement, the chamber was vented to air again and the sample was further annealed. The accumulative annealing time was up to 2.5 h. The integrated peak intensity and full width at half maximum (FWHM) of diffraction peaks were used to evaluate the oxidation of the samples. The scanning step was 0.001° and accumulation time was 3 s at each step. The procedure was further repeated to accumulate the desired anneal time.

**Table 1.** Intensity and FWHM for (400) and (511) peaks of magnetite (100) with and without an Au overlayer and calculated cap layer thickness.

| | $Fe_3O_4$ | | $Au/Fe_3O_4$ | | |
|---|---|---|---|---|---|
| Diffraction peak | Integrated intensity | FWHM (deg) | Integrated intensity | FWHM (deg) | Calculated cap layer thickness (nm) |
| (400) | 373.8 | 0.0465 | 20.1 | 0.0547 | 1337 |
| (511) | 187.5 | 0.0509 | 6.79 | 0.0458 | 1325 |

X-ray powder diffraction (powder XRD) (Siemens DACO_MP) and Raman spectroscopy (RS) (Renishaw) measurements were carried out to clarify the thermal annealing induced phase on the magnetite surface before and after annealing.

## 3. Results and discussion

In order to verify the validity of equation (1), an Au film with a thickness of 1300 nm was deposited on a magnetite (100) single-crystal surface using magnetron sputtering. The specimen was covered by a mask in such a way that only half of the sample surface was covered by the Au film. Symmetric $\omega$–$2\theta$ scans of the (400) diffraction peak and asymmetric $\omega$–$2\theta$ scans of the (511) diffraction peak were performed on bare and Au-coated magnetite (100) surfaces respectively by means of HRXRD. A value of $\mu = 4006.4\ \mathrm{cm}^{-1}$ for the linear absorption coefficient of gold was used [18]. According to equation (1), the thickness of the Au layer was calculated based on experimental data for the (400) and (511) crystallographic planes using symmetric and asymmetric diffraction respectively. The results are shown in table 1 along with the measured intensity and FWHM. The calculated results agree well with the expected value of 1300 nm.

To establish what oxide phase was formed on the three magnetite surfaces, the following experiment was performed. The single crystals were annealed at 300 °C for up to 150 min at ambient air pressure and symmetric $\omega$–$2\theta$ scans were then performed on powder XRD. The representative results for the three surfaces, (100), (110) and (111), are shown in figures 3(a)–(c) respectively. $\alpha$-$Fe_2O_3$ was clearly formed on all three surfaces. We can also confirm that no traces of any other iron oxide phases were detected. The specimens which were annealed in air for a much shorter time, e.g. 0.25 h also show formation of the $\alpha$-$Fe_2O_3$ phase. On the (100) and (111) surfaces the layer of $\alpha$-$Fe_2O_3$ was not epitaxial because of the appearance of diffraction peaks from the $\alpha$-$Fe_2O_3$ layer. In the case of the (110) surface, even though there is only one diffraction peak from the cap layer ($\alpha$-$Fe_2O_3$), the cap layer is unlikely to be epitaxial because of the difference between the in-plane atomic termination of $Fe_3O_4(110)$ and $\alpha$-$Fe_2O_3(\bar{2}11)$ plane.

It has been reported [1] that $\alpha$-$Fe_2O_3(001)$ can grow epitaxially on magnetite (111). However, we did not observe any evidence of epitaxial growth. Raman spectroscopy results confirm the powder XRD data (figure 4). After annealing the magnetite (100) at 250 °C for 2 h, the intensity of the $Fe_3O_4$ peaks at 540 and 303 $\mathrm{cm}^{-1}$ was significantly reduced and new peaks corresponding to $\alpha$-$Fe_2O_3$ become visible. The main magnetite peak, at 668 $\mathrm{cm}^{-1}$, was still dominant. When the annealing temperature was increased to 300 °C, the $\alpha$-$Fe_2O_3$ peaks became the most intense peaks in the spectrum. This suggests that $\alpha$-$Fe_2O_3$ is the dominant phase in the subsurface layer and that the subsurface layer is at least several hundred nanometres thick, which is the typical penetration depth of the RS laser used to investigate the sample.

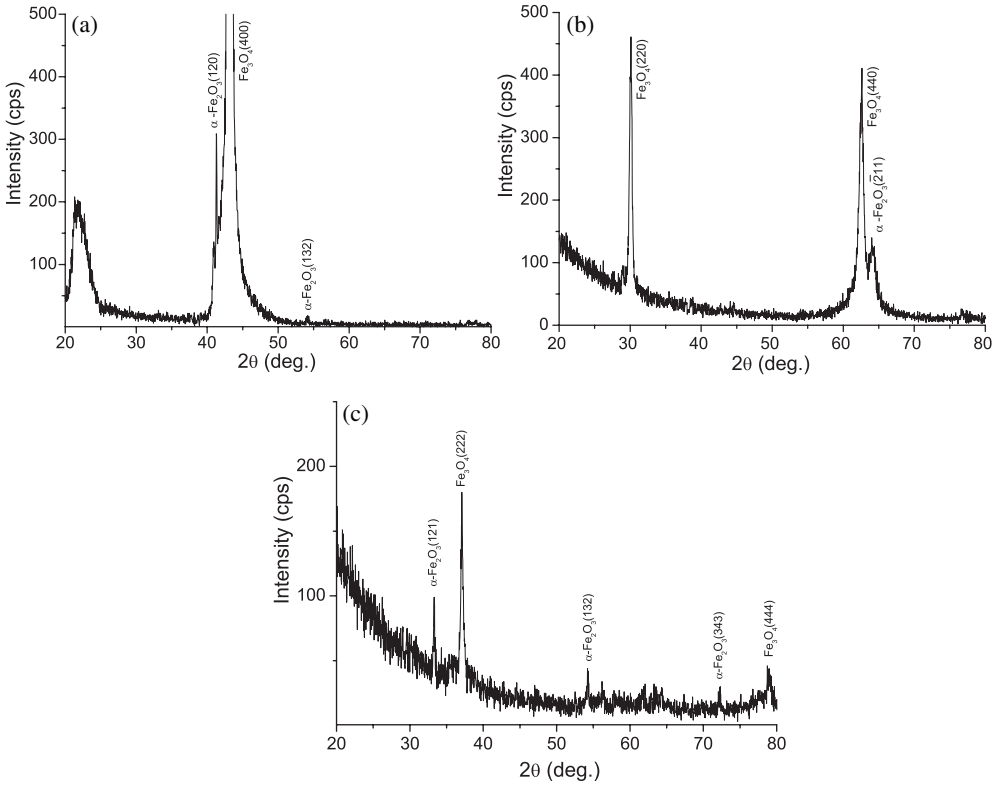


**Figure 3.** The XRD $\omega$–$2\theta$ patterns of magnetite single crystals (a) (100), (b) (110) and (c) (111) surfaces all annealed in air at 300 °C.

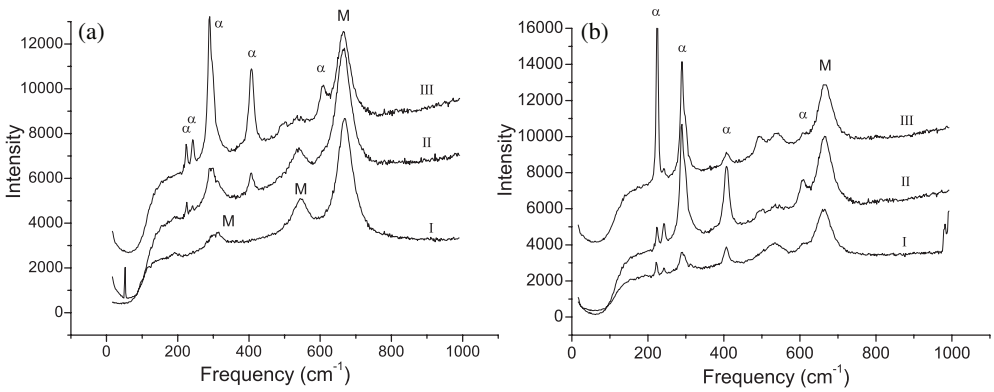


**Figure 4.** Raman spectra of (a) magnetite (100) surface annealed, curves I, II and III correspond to as-polished sample, sample annealed at 250 °C for 2 h and sample annealed at 300 °C for 2.4 h, respectively. (b) Magnetite (111), (100) and (110) surfaces annealed in air at 300 °C represented by curves I, II and III respectively. Peaks corresponding to $Fe_3O_4$ and $\alpha$-$Fe_2O_3$ are marked with letters M and $\alpha$, respectively.

Figure 5 shows the dependence on the annealing time of the normalized integrated intensity and FWHM of the symmetric (400) diffraction peak obtained from HRXRD for $Fe_3O_4$(100) for an annealing temperature of 250 °C. As expected the intensity of the (400) diffraction

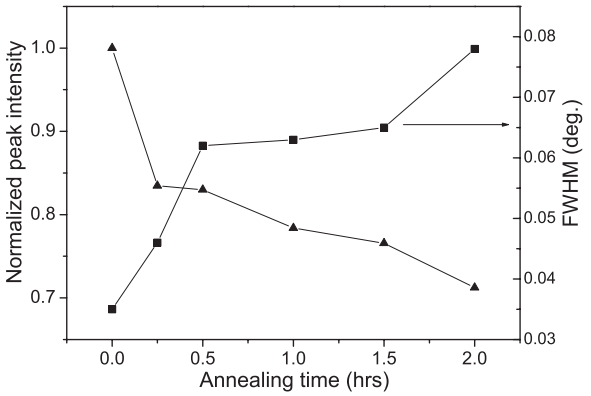


**Figure 5.** The dependence on the annealing time of the normalized integrated intensity and FWHM for the (400) diffraction peak for $Fe_3O_4(100)$ surface annealed at 250 °C.

peak decreases and the peak broadens with increasing annealing time. On the contrary, at this annealing temperature the $Fe_3O_4(110)$ and (111) surfaces did not show any appreciable change in peak intensity, even for an annealing time of up to 1 h. These results imply that the oxidation kinetics is dependent on the crystallographic orientation of the surface making the $Fe_3O_4(100)$ crystal surface more reactive than the (110) and (111) ones.

The dependence of the integrated intensity of the symmetric (400), (440) and (222) diffraction peaks on the annealing time for $Fe_3O_4(100)$, (110) and (111) respectively is shown in figure 6. The annealing temperature in this experiment was 300 °C. It was found that the peak intensity for the $Fe_3O_4(100)$ surface decreases much faster than for the other two surfaces. Figure 7 shows the dependence of the FWHM for the symmetric (400), (440) and (222) diffraction peaks on the annealing time for $Fe_3O_4(100)$, (110) and (111) respectively, for an annealing temperature of 300 °C. It was found that the FWHM for all three magnetite surfaces increased with annealing time. The broadening of the diffraction peaks indicates the development of a distribution of lattice parameter values caused by strain. With annealing, iron cations diffuse to the surface and form the cap layer of $\alpha$-$Fe_2O_3$. Then below the cap layer, vacancy defects are left because of the iron cation movement. Gallagher *et al* [8] investigated broadening of XRD peaks during oxidation in quenched powder samples and attributed the broadening to the variation of the lattice parameter with the concentration gradient. Strain that develops in $Fe_3O_4$ when $\alpha$-$Fe_2O_3$ layers form on top of it is also contributes to the increase in FWHM.

The thickness of the cap layer ($\alpha$-$Fe_2O_3$) induced by annealing of the magnetite surface was calculated using equation (1). The value of $\mu = 5980\ \mathrm{cm}^{-1}$ for the linear absorption coefficient of $\alpha$-$Fe_2O_3$ was calculated using the values of mass absorption coefficients for iron and oxygen [18]. Figure 8 shows values of the cap layer thickness as a function of annealing time at 250 °C, calculated from the experimental data and also a power-law fit for the (100) surface. Figure 9 shows similar results for $Fe_3O_4(100)$, (110) and (111) annealed at 300 °C as a function of time. In order to study the mechanism and rate of oxidation, we employed the following fitting equation:

$$x = A(\tau/\tau_0)^n, \tag{2}$$

where $x$ is the oxide thickness in nanometres, $\tau$ is the annealing time in hours, $\tau_0$ is a constant taken to be 1 h arbitrarily, $A$ can be regarded as an oxidation rate factor and $n$ is the power-law coefficient. The selection of $\tau_0$ will influence the absolute value of fitted $A$ only and has

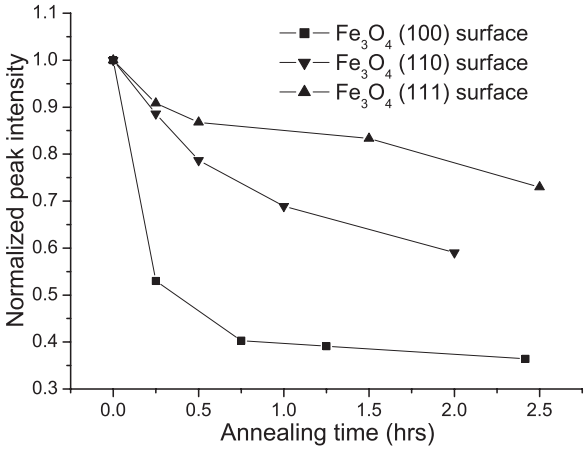


**Figure 6.** The dependence on the annealing time of the integrated intensity of the symmetric (400), (440) and (222) diffraction peaks for $Fe_3O_4$(100), (110) and (111) surfaces respectively. The annealing temperature is 300 °C.

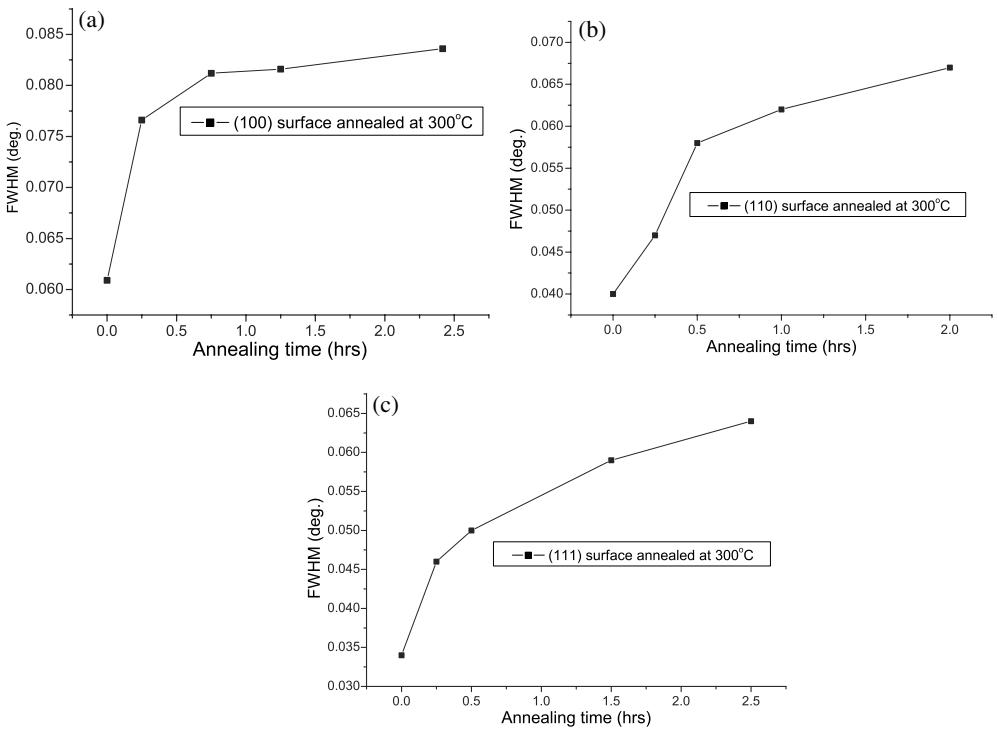


**Figure 7.** Dependence on the annealing time of FWHM of the (400), (440) and (222) diffraction peaks for magnetite (a) (100), (b) (110) and (c) (111) surface respectively.

no effect on the value of fitted $n$. This is clear if one rewrites equation (2) as $x = A^*(\tau)^n$ where $A^* = A/\tau_0^n$. Table 2 summarizes parameters obtained from the fitting procedure. For annealing temperatures up to 300 °C, the value of $A$ is greatest for the (100) surface. Normally, $n$ determines the mechanism of the oxidation kinetics [19, 20]. The value of $n$ for the magnetite

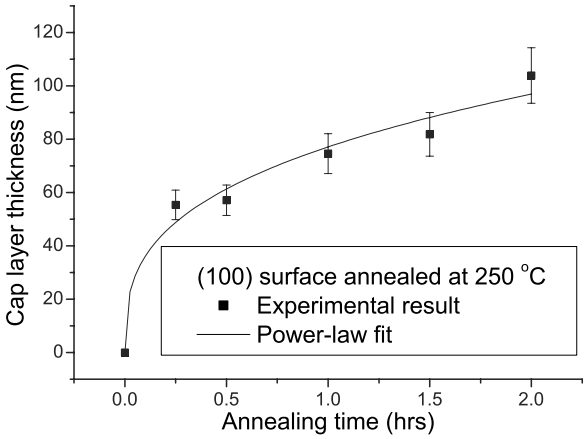


**Figure 8.** Experimental data and power-law fit for the thickness of the cap layer as a function of anneal time at 250 °C for the magnetite (100) surface.

**Table 2.** The parameters used to fit the cap layer thickness.

| | $A$ (nm) | $n$ |
|---|---|---|
| $Fe_3O_4$(100) annealed at 250 °C | $77.1 \pm 2.9$ | $0.33 \pm 0.07$ |
| $Fe_3O_4$(100) annealed at 300 °C | $271.6 \pm 8.3$ | $0.19 \pm 0.04$ |
| $Fe_3O_4$(110) annealed at 300 °C | $152.2 \pm 5.4$ | $0.62 \pm 0.05$ |
| $Fe_3O_4$(111) annealed at 300 °C | $48.8 \pm 4.5$ | $0.50 \pm 0.12$ |

(100) surface ($0.19 \pm 0.04$) is quite different from the other two orientations (110) and (111) ($0.62 \pm 0.05$ and $0.50 \pm 0.12$ respectively). It could therefore be suggested that the mechanism of oxidation from $Fe_3O_4$ to $\alpha$-$Fe_2O_3$ for different crystal planes is different. $n$ is $0.50 \pm 0.12$ for magnetite (111) which agrees with the value expected on the basis of the $t^{0.5}$ law from Wagner's theory [19]. For magnetite (110) $n$ is $0.62 \pm 0.05$, which still closely agrees with the expected value from Wagner's theory. $n$ is $0.19 \pm 0.04$ for the magnetite (100) surface which implies that Wagner's model is not the main mechanism for the oxidation of the magnetite (100) surface. It should be recalled that Wagner's theory assumes that space charge effects are negligible; the rate-controlling step is the volume diffusion of ions. There could be other mechanisms such as electric field assisted cation diffusion, electric diffusion and electron tunnelling contributing to the oxidation of the magnetite (100) surface [19, 20].

Clearly, our results suggest that the cation diffusion constant is greater along the (100) direction than along either the (111) or (110) direction; however, in our view this factor alone does not describe the differences between the oxidation kinetics of the three low-index surfaces. This is explained in detail below. One could expect that in an oxide, both the diffusion of anions (oxygen) and cations (iron) affect the oxidation of the crystal and should be taken into account. It is known, however [11, 12], that in magnetite the oxidation mechanism based on the diffusion of iron cations, oxygen is adsorbed and ionized with electrons coming from the transformation of $Fe^{2+}$ to $Fe^{3+}$. This oxidation should cause a diffusion of iron ions from the bulk of the crystal towards the surface. Thus, the oxidation of magnetite is mainly influenced by the diffusion of iron cations. One can appreciate that for the formation of $\alpha$-$Fe_2O_3$ on the magnetite surface, the diffusion of cations through both the bulk $Fe_3O_4$ and the existing cap layer of $\alpha$-$Fe_2O_3$ is necessary. The self-diffusion of iron in magnetite as a

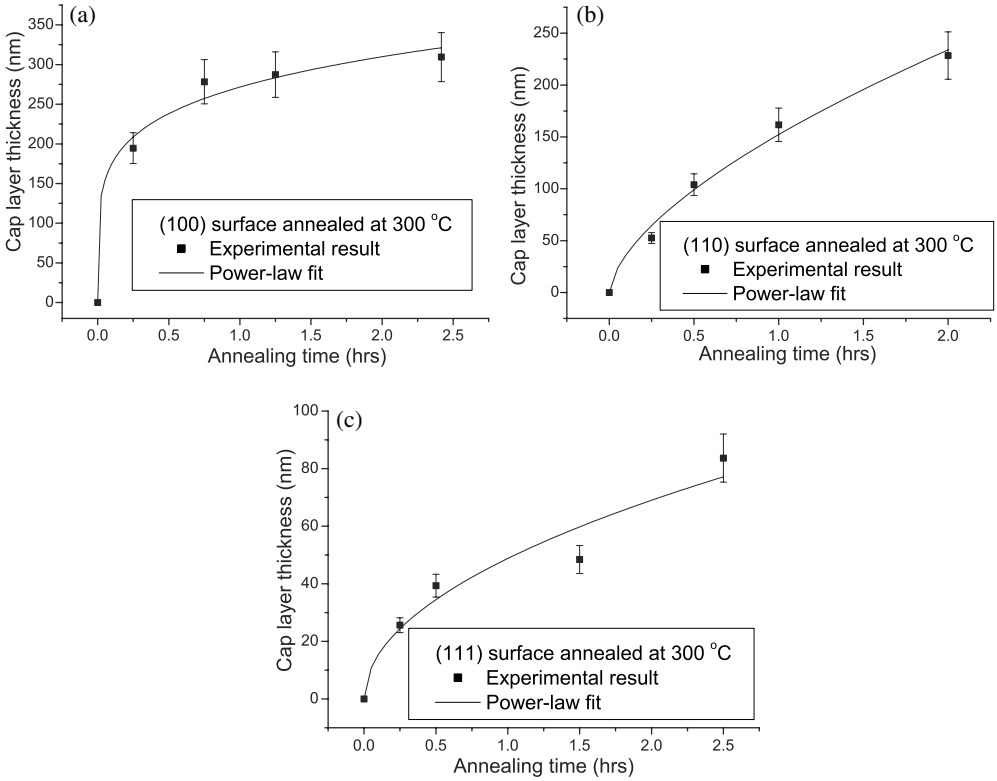


**Figure 9.** Experimental data and power-law fit for the thickness of the cap layer for (a) magnetite (100), (b) (110) and (c) (111) surface, respectively, as a function of annealing time at 300 °C.

function of oxygen pressure has been studied in the temperature range 900–1400 °C [21, 22]. Near the wüstite/magnetite interface where interstitial cations predominate as defects, the iron self diffusion coefficient is proportional to $PO_2^{-2/3}$. At the magnetite/haematite interface, where iron vacancies predominate, the self-diffusion coefficient is proportional to $PO_2^{2/3}$. Previous studies [21, 22] did not deal with the dependences of the self-diffusion on the crystal orientation. On the other hand it has been reported [23, 24] that the iron self-diffusion in $\alpha$-$Fe_2O_3$ is extremely slow. One can therefore consider the oxidation of magnetite as a two-stage process. In the early stage, the self-diffusion of iron through the magnetite single crystal is the critical factor and it is dependent on the crystal orientation. With further annealing, as the thickness of the $\alpha$-$Fe_2O_3$ layer increases, oxygen could diffuse down to the $\alpha$-$Fe_2O_3$/$Fe_3O_4$ interface and iron cations could diffuse to the surface through the $\alpha$-$Fe_2O_3$ layer. Prior works [11, 12] suggested that the diffusion of iron cations is the main mechanism during the oxidation of magnetite. The iron cations have a much smaller diameter than oxygen anions. The diffusion of iron cations will most likely be much faster than that of oxygen anions. Thus, the diffusion of iron cations is thought to be the controlling factor during the oxidation. Because of the extremely slow diffusion of iron in $\alpha$-$Fe_2O_3$, the self-diffusion of iron through $\alpha$-$Fe_2O_3$ becomes the limiting factor. As the layer of $\alpha$-$Fe_2O_3$ does not grow epitaxially on the surface of $Fe_3O_4$, defects must be formed in the cap layer of haematite that allow faster migration of oxygen anions and iron cations. The density of defects should be different for the three low-index surfaces. One could expect that the density and the type of

defect formed in the layer of $\alpha$-$Fe_2O_3$ is the factor defining the dynamics in the later stages of oxidation. It should be pointed out that a relative humidity change can dramatically change the oxidation rates on some materials. The reaction of water with the (100) and (111) surfaces of $Fe_3O_4$ was investigated [25], and the results indicate that reaction rates are similar and thus do not appear to depend on surface orientation. The hydroxylation reaction rate is not sensitive to the water vapour pressure when it is in the range of several millibars which is similar to our experimental environment. Considering these factors, the humidity is not likely to have a pronounced effect on our experimental results.

## 4. Conclusions

This study has demonstrated that HRXRD using an *in situ* hot stage is an effective technique for the investigation of nanometre range oxidation kinetics. The intensity of the (400) diffraction peaks on the magnetite (100) surface decreases and the FWHM increases with annealing at 250 °C. For $Fe_3O_4$(110) and (111) crystals no clear peak intensity change was observed up to an annealing time of 1 h at 250 °C. A reduction in the intensity of the diffraction peaks was observed for all three magnetite crystal planes when the samples were annealed at 300 °C. The diffraction peaks become broadened with increased annealing time which results from vacancy defects and the development of strain consistent with the formation of the $\alpha$-$Fe_2O_3$ layer. The parameters of oxidation kinetics for magnetite were obtained through a fitting procedure. It is found that the oxidation rate for magnetite (100) is greater than that for (110) and (111). The oxidation mechanisms for these three orientations are different. The oxidation of the magnetite (111) and (110) surfaces followed Wagner theory; however, the oxidation of magnetite (100) does not. It is considered that other mechanisms such as electric field assisted cation diffusion, electric diffusion and electron tunnelling may contribute to the oxidation of the magnetite (100) surface. As the density of defects is thought to depend on the magnetite surface termination, the rate of oxidation for different low-index surfaces must differ.

## Acknowledgment

This work was supported by Science Foundation Ireland (SFI) under the contract of 00/PI.1/C042.

## References

[1] Cornell R M and Schwertmann U 1996 *The Iron Oxides* (Weinheim: VCH)
[2] Alvarado S F, Erbudak M and Munz P 1976 *Phys. Rev.* B **14** 2740
[3] Bratkovsky A M 1997 *Phys. Rev.* B **56** 2344
[4] Coey J M D, Berkowitz A E, Balcells L, Putris F F and Parker F T 1998 *Appl. Phys. Lett.* **72** 734
[5] Mariotto G, Murphy S and Shvets I V 2002 *Phys. Rev.* B **66** 245426
[6] Shvets I V, Berdunov N, Murphy S and Mariotto G 2003 *Europhys. Lett.* **63** 867
[7] Xu X N, Wolfus Y, Shaulov A, Yeshurun Y, Felner I, Nowik I, Koltypin Yu and Gedanken A 2002 *J. Appl. Phys.* **91** 4611
[8] Gallagher P K, Gyorgy E M and Bair H E 1979 *J. Chem. Phys.* **71** 830
[9] Colombo U, Gagherazzi G, Gazzarrini F, Lanzavecchia G and Sironi G 1964 *Nature* **202** 175
[10] Colombo U, Gazzarrini F, Lanzavecchia G and Sironi G 1965 *Science* **147** 1033
[11] Gallagher K J, Feitknecht W and Mannweiler U 1968 *Nature* **217** 1118
[12] Feitknecht W and Gallagher K J 1970 *Nature* **228** 548
[13] Caudron E and Buscail H 2001 *Corros. Sci.* **43** 1477
[14] Schimanke G and Martin M 2000 *Solid State Ion.* **136/137** 1235
[15] DeBoer F E and Selwood P W 1954 *J. Am. Chem. Soc.* **76** 3365

[16] Stierle A and Zabel H 1997 *Surf. Sci.* **385** 167
[17] Muralidharan G, Wu X Z, You H, Paulikas A P and Veal B W 1997 *Scr. Mater.* **37** 1177
[18] Cullity B D and Stock S R 2001 *Elements of X-Ray Diffraction* (Upper Saddle River, NJ: Prentice-Hall)
[19] Kofstad P 1988 *High-Temperature Corrosion* (London: Elsevier)
[20] Cabrera A L, Sales B C and Maple M B 1982 *Phys. Rev.* B **25** 1688
[21] Dieckmann R and Schmalzried H 1978 *Ber. Bunsenges. Phys. Chem.* **39** 344
[22] Dieckmann R 1978 *Ber. Bunsenges. Phys. Chem.* **86** 112
[23] Kingery W D, Hill D C and Nelson R P 1960 *J. Am. Ceram. Soc.* **43** 1473
[24] Reddy K P R and Cooper A R 1983 *J. Am. Ceram. Soc.* **66** 664
[25] Kendelewicz T, Liu P, Doyle C S, Brown G E Jr, Nelson E J and Chambers S A 2000 *Surf. Sci.* **453** 32